MIT Open Access Articles

Crystal structures of asymmetric ClpX hexamers reveal nucleotide-dependent motions in a AAA+ protein-unfolding machine

Crystal structures of asymmetric ClpX hexamers reveal nucleotide-dependent motions in a AAA+ protein-unfolding machine

Steven E. Glynn[1], **Andreas Martin**[1], **Andrew R. Nager**[1], **Tania A. Baker**[1,2], and **Robert T. Sauer**[1,*]

[1]Department of Biology Massachusetts Institute of Technology, Cambridge, MA 02139 USA

[2]Howard Hughes Medical Institute Massachusetts Institute of Technology, Cambridge, MA 02139 USA

Summary

ClpX is a AAA+ machine that uses the energy of ATP binding and hydrolysis to unfold native proteins and translocate unfolded polypeptides into the ClpP peptidase. The crystal structures presented here reveal striking asymmetry in ring hexamers of nucleotide-free and nucleotide-bound ClpX. Asymmetry arises from large changes in rotation between the large and small AAA+ domains of individual subunits. These differences prevent nucleotide binding to two subunits, generate a staggered arrangement of ClpX subunits and pore loops around the hexameric ring, and provide a mechanism for coupling conformational changes caused by ATP binding or hydrolysis in one subunit to flexing motions of the entire ring. Our structures explain numerous solution studies of ClpX function, predict mechanisms for pore elasticity during translocation of irregular polypeptides, and suggest how repetitive conformational changes might be coupled to mechanical work during the ATPase cycle of ClpX and related molecular machines.

Keywords

energy-dependent degradation; ClpXP; protein unfolding; AAA+ molecular machines

AAA+ molecular machines use the energy of ATP binding and hydrolysis to power the degradation, remodelling, disassembly, or movement of macromolecular complexes in a wide variety of cellular processes (Hanson and Whiteheart, 2005; White and Lauring, 2007). *E. coli* ClpX is a hexameric AAA+ protein-unfolding machine, which can function alone or with the ClpP peptidase (Levchenko et al., 1997; Grimaud *et al.*, 1998). In the ClpXP protease, a ring hexamer of ClpX mediates ATP-dependent unfolding of specific proteins, for example those bearing the 11-residue ssrA tag, and then translocates the denatured polypeptide into the lumen of ClpP for degradation (Fig. 1A; Gottesman et al., 1998; Kim et al., 2000; Singh et al., 2000). ClpX can also unfold proteins with specific recognition tags in the absence of ClpP (Kim et al., 2000). Each subunit of the ClpX hexamer is identical in sequence and consists of

*Correspondence: bobsauer@mit.edu.

large and small AAA+ domains and a family-specific N-domain (Fig. 1B; Schirmer et al., 1996). However, variants lacking the N-domain (ClpX-ΔN) can still combine with ClpP to mediate efficient degradation of native ssrA-tagged proteins (Singh et al., 2001; Wojtyra et al. 2003). Structures of the large and small AAA+ domains are known for a subunit of *Helicobacter pylori* ClpX-ΔN, but these subunits do not form hexamers in the crystal, assembling instead into helical filaments that span the lattice (Kim and Kim, 2003).

The axial pore of the ClpX hexamer serves as the translocation channel into ClpP (Fig. 1A; Ortega et al., 2000). Moreover, three different pore loops – called "GYVG", "pore-2", and "RKH" – play roles in binding the ssrA tag (Siddiqui et al., 2004; Farrell et al., 2007; Martin et al., 2007; 2008a; 2008b). In addition, some of these loops also mediate binding to and communication with ClpP and are needed for protein unfolding and/or translocation. For example, current models suggest that the GYVG loops grip polypeptide substrates and then pull or drag these molecules into the pore as a consequence of nucleotide-dependent loops movements (Martin et al., 2008b). This pulling mechanism could generate a force to unfold native substrates that cannot enter the pore and provide a way to translocate the polypeptide once unfolding occurs. It is not known if these GYVG-loop movements occur in a localized fashion or as part of larger domain or subunit motions. Importantly, ClpX can translocate radically different polypeptides, including homopolymeric blocks of large, small, charged, or hydrophobic amino acids, as well as unnatural sequences with additional methylene groups between successive peptide bonds (Barkow et al., 2009). Moreover, ClpX can translocate disulfide-bonded proteins, which requires simultaneous passage of three polypeptide chains through the axial pore (Burton et al., 2001; Bolon et al., 2004). How the ClpX pore mediates transport of such diverse polypeptide substrates is not known.

ATP binding and hydrolysis fuel protein unfolding and translocation by ClpX. In principle, a ClpX hexamer could bind six ATPs, but solution experiments with saturating ATP show that at least two subunits remain nucleotide free (Hersch *et al.*, 2005). Moreover, these studies reveal a minimum of two classes of ATP-binding subunits that differ in the kinetics of nucleotide release. In addition, single-chain ClpX hexamers with covalently linked subunits retain the ability to unfold and translocate substrates efficiently, even when only a few subunits are able to hydrolyze ATP (Martin *et al.*, 2005). These results suggest that ClpX hexamers function asymmetrically, with specific subunits assuming distinct conformations and roles during the ATPase cycle. A related hexameric unfoldase, HslU, also appears to bind a maximum of four ATPs in solution (Yakamavich et al., 2008). Curiously, however, completely symmetric crystal structures of the HslU hexamer with six bound nucleotides have been reported, and even HslU structures with just three or four bound nucleotides show only modest deviations from six-fold rotational symmetry (Bochtler et al., 2000; Sousa et al., 2000; 2002; Wang et al., 2001; Kwon et al., 2003). Hence, it is uncertain whether ClpX hexamers adopt structures that are substantially asymmetric.

Understanding how ClpX and related AAA+ enzymes function will require information about the conformational states that these machines adopt during the coupled ATPase and mechanical cycles (Tucker and Sallai, 2007). Here, we report crystal structures of nucleotide-free and nucleotide-bound ClpX hexamers, which are strikingly asymmetric because of differences in rotation between the large and small AAA+ domains of individual subunits. These differences generate a staggered arrangement of subunits and pore loops around the hexameric ring, result in two subunits that cannot bind nucleotide, and provide a mechanism for transmitting structural changes caused by ATP binding or hydrolysis in one subunit to neighboring subunits and to the entire ring. Our structures suggest a mechanism of pore elasticity that would allow expansion to accommodate multiple polypeptides or substrates with large side chains and contraction to maintain contact with polypeptides consisting of small amino acids. Finally,

these structures suggest plausible rigid-body conformational changes that could power protein unfolding and polypeptide translocation.

Results

Crystallization

Several factors influenced our choice of a ClpX variant to use for crystallization. We sought to improve solubility by deleting the N domain and to use mutations that prevent ATP hydrolysis and/or mimic the functional asymmetry observed in the wild-type hexamer. The variant crystallized contained three *E. coli* ClpX-ΔN subunits connected by flexible linkers, which are compatible with function (Fig. 1B; Martin et al., 2005). Moreover, each subunit contained an E185Q mutation in the Walker-B motif to block ATP hydrolysis (Hersch *et al.*, 2005), and the sensor-II motif of the third subunit contained an R370K mutation, which allows nucleotide binding but blocks ATP-dependent conformational changes and thus mimics an ATP-free state (Joshi et al., 2004). This pseudo-trimer bound ClpP and an ssrA peptide in an ATP-dependent manner (not shown), establishing that it can dimerize to form a pseudo-hexamer and adopt functional conformations, similar to the wild-type ClpX hexamer.

An initial crystal form (space group $P2_12_12_1$; a = 63.3 Å, b = 199.9 Å, c = 202.5 Å) was obtained using ammonium sulfate as the precipitant. This form grew in the absence of nucleotide, had a single ClpX pseudo-hexamer in the asymmetric unit, and diffracted to 4.0 Å resolution for the best crystals. When these crystals were soaked in mother liquor plus $MgCl_2$ and nucleotide (ATP, ATPγS, or ADP), the unit-cell shrank substantially (a = 54.1 Å, b = 178.5 Å, c = 201.4 Å). Unit-cell changes were not observed in soaking experiments without nucleotide. Although unit-cell shrinkage was detected in crystals soaked for 2 min or less, the best data were obtained from a crystal soaked in ATPγS for 12 h, which diffracted to 3.25 Å resolution. Phases were initially obtained by molecular replacement, and structures were refined to R_{work}/R_{free} values of 0.27/0.31 for the nucleotide-free crystal and 0.24/0.28 for the ATPγS-soaked crystal (Table 1). The electron-density maps were of sufficient quality to trace the main chain and to position most side chains (Fig. 1C). There were clear differences in the two hexameric structures, reflecting nucleotide-dependent motions.

Asymmetric ring hexamers

ClpX formed an asymmetric ring hexamer in both the nucleotide-free and nucleotide-bound structures, with ring diameters and heights (Fig. 1D, 1E) that were generally consistent with those estimated by electron microscopy of *E. coli* ClpX-ΔN (Singh *et al.*, 2001). However, the crystallographic hexamers were strikingly different from the 6-fold symmetric molecule observed in averaged EM images and from a structure modeled using an HslU hexamer to define the quaternary arrangement of subunits (Grimaud *et al.*, 1998; Kim and Kim, 2003). In a 6-fold symmetric ring hexamer, the corresponding atoms of all six subunits lie in planes perpendicular to the symmetry axis. By contrast, the axial positions of equivalent amino acids in the ClpX small AAA+ domains (residues 320-416) were staggered in both the nucleotide-bound and nucleotide-free hexamers (Fig. 1E). Non-planarity of equivalent residue positions in different subunits was also observed in the large AAA+ domains (residues 61-314) and in the linkers (residues 315-319) that connect the two domains. The covalent tethers between subunits were not observed in electron-density maps. In both crystallographic hexamers, an axis of approximate 2-fold rotational symmetry related the A/B/C and D/E/F subunit groups (Fig. 1D), producing an inexact dimer of trimers (rmsd 1.8 Å) in which some pseudo-symmetric subunits had noticeable differences in structure.

Structural origins of asymmetry

Superposition of the large AAA+ domains from the 12 subunits in both ClpX hexamers revealed very similar backbone conformations (rmsd < 0.8 for Cα atoms). The folds of the small AAA+ domains were also essentially identical (rmsd < 0.35 Å). Hence, structural changes in the interfaces between different subunits or between different domains in the same subunit must generate the asymmetry within hexamers and the conformational rearrangements that occur between nucleotide-free and nucleotide-bound hexamers.

Strikingly, distinct types of subunits were present in both ClpX hexamers. We define two general classes based on the orientations of the large and small AAA+ domains, which is determined by differences in the inter-domain linker conformation. The rotation between domains in type-1 subunits (A/B/D/E in both hexamers) creates a conformation compatible with nucleotide binding in the inter-domain cleft, whereas rotations between domains in type-2 subunits (C/F in both hexamers) result in a conformation that destroys the nucleotide-binding pocket (see Fig. 3B). The differences between type-1 and type-2 subunits are dramatic. For example, the rotations between domains in the most divergent type-1 and type-2 subunits differ by 82° (Fig. 1F). Moreover, after superposition of the large AAA+ domains of type-1 and type-2 subunits, equivalent residues in the attached small AAA+ domains can occupy positions more than 30 Å apart.

Two interfaces, one highly conserved and one highly variable, contribute to the packing between neighboring subunits in the ClpX ring. The major interface is formed by the packing of each small AAA+ domain against the large AAA+ domain of the clockwise subunit (in the top view of Fig. 1D). This interface buries an average of approximately 2000 Å^2 of surface area, and superposition of the large domains from any two subunits results in very similar positions of the neighboring small domains (Fig. 2A). In other words, adjacent small and large AAA+ domains can be viewed as a single rigid-body unit, and the hexamer comprises six such units (Fig. 2B). Changes in rotation between the large and small AAA+ domains of a single monomer propagate via the rigid-body interfaces and affect the orientation of the adjacent large AAA+ domain. The less conserved subunit interfaces occur between adjacent large AAA+ domains and show substantial variations in orientation, packing geometry, and surface burial (340-1340 Å^2). For example, large domains clockwise from type-1 versus type-2 subunits have very different orientations (Fig. 2C).

Closing the hexameric ring

The topologically closed rings of both crystallographic hexamers showed a 1-1-2-1-1-2 pattern of type-1 and type-2 subunits (Fig. 3A). A hexamer modeled using only type-1 subunits and the major subunit interface had a lock-washer conformation in which the first and sixth subunits were not in contact. A similar arrangement of subunits occurs in the helical filaments seen in *H. pylori* ClpX crystals (Kim and Kim, 2003). Similarly, modeling showed that closed rings could not be constructed from type-2 subunits alone. Thus, a mixture of type-1 and type-2 subunits appears to be required to form a closed ClpX ring.

Nucleotide binding

Our structures provide a straightforward explanation for the finding that ClpX hexamers bind a maximum of four ATP molecules in solution (Hersch et al., 2005). In AAA+ enzymes, ATP/ADP binds at the interface between the large and small AAA+ domains of one subunit and the large AAA+ domain of an adjacent subunit (Erzberger and Berger, 2006), creating six potential binding sites. In ClpX, however, only four sites can bind ATP/ADP (Fig. 3A), because the small domain in type-2 ClpX subunits occupies the space where nucleotide would normally bind (Fig. 3B). In type-1 subunits, by contrast, the adenine base of a nucleotide can interact

with the short linker between the large and small domains (Fig. 3B), providing a mechanism to link binding to structural changes in hexamer conformation.

After soaking a nucleotide-free crystal in ATPγS overnight, we observed full occupancy of the nucleotide-binding sites in subunit A and B, partial occupancy in subunit E, and low occupancy in subunit D. These differences could result from affinity differences in the crystal or from different rates of nucleotide binding, as a partially refined structure of a crystal soaked in ATPγS for 30 min showed nucleotide density only in subunit A. We observed similar changes in unit-cell dimensions after soaking crystals in ATPγS, ATP, or ADP, suggesting that the changes observed with the nucleoside triphosphates might be driven by binding of ADP, present either as a contaminant or produced by hydrolysis in the crystal. Indeed, ADP fit the electron-density in the ATPγS-soaked crystal best (Fig. 3B), although we are not confident of this assignment at the resolution of this structure.

A sulfate molecule was observed in the malformed pockets of the type-2 C and F subunits in the nucleotide-bound crystal and in all pockets of the nucleotide-free crystal. These sulfates occupy sites where the β-phosphate of a nucleoside triphosphate would normally be expected and may mimic some aspects of nucleotide binding.

Motions driven by nucleotide binding

Nucleotide binding has two consequences. First, the orientation of the large and small domains of type-1 subunits changes. For example, rotation between the large and small domains of subunit A increased by 15° after nucleotide binding, whereas these domains in subunit B rotated by 14° in the opposite direction (Fig. 3C). Second, these rotations result in a complex set of motions of the associated rigid-body units, as shown by overlays of the structures of nucleotide-free and nucleotide-bound hexamers (Fig. 4). In units with a type-1 small domain, this domain moves downward and inward towards the bottom face of the hexamer, whereas its partner large domain moves upward and inward, closing the pore. In units with a type-2 small domain, the entire rigid-body element moves up and away from the pore. These combined motions cause a significant flexing of the ClpX hexamer in the plane of the ring, resulting in a nucleotide-bound structure that is taller, narrower, and has a more constricted pore than the nucleotide-free structure. Detailed motions can also be seen in movies available in Supplementary Materials.

Axial staggering of pore loops

The GYVG and pore-2 loops project into the lumen of the axial pore, whereas the RKH loops surround the upper entry to the pore. All of these ClpX loops play roles in binding of the ssrA degradation tag of substrates, and subsets mediate translocation, unfolding, and dynamic contacts with ClpP (Siddiqui et al., 2004; Farrell et al., 2007; Martin et al., 2007; 2008a; 2008b). The electron-density maps were of sufficient quality to place the GYVG loops (residues 152-155) in all subunits of the nucleotide-bound hexamer and many of the subunits in the nucleotide-free structure. Large sections of the pore-2 loops (residues 191-201) could be confidently built in several subunits of the nucleotide-bound structure. Although the remaining pore-2 loops and all RKH loops (residues 222-236) were disordered, we could place them approximately based upon connections to well-ordered structural elements. For each type of pore loop, we observed or inferred substantial staggering relative to the pore axis when equivalent loops in neighboring subunits were compared (Fig. 5). For example, viewing the nucleotide-bound hexamer perpendicular to the pore axis, the GYVG loop of subunit A is close to the bottom of the pore, the GYVG loop of the adjacent type-1 subunit B occupies an intermediate position, and the GYVG loop of the neighboring type-2 subunit F is closer to the top of the pore (Fig. 5A).

Discussion

The crystal structures presented here reveal dramatically asymmetric conformations for the hexameric ring of ClpX both in nucleotide-bound and nucleotide-free states. We note several important architectural principles. (*i*) Although all six subunits of the hexamer have the same sequence and essentially identical folds for the large and small AAA+ domains, differences in orientation between the large and small AAA+ domains of individual subunits define two general classes of subunits. Type-1 subunits bind nucleotide, whereas type-2 subunits do not. (*ii*) The major interface between subunits is formed by the packing of a small AAA+ domain against the neighboring large AAA+ domain. Because this interface is structurally conserved, this unit moves as a rigid body around restricted swivel points defined by the conformations of the linkers in adjacent subunits. (*iii*) The topologically closed hexameric ring is formed by a 1-1-2-1-1-2 pattern of type-1 and type-2 subunits, which results in substantial staggering of domains and structural elements with respect to the central pore axis. (*iv*) Nucleotide binding to type-1 subunits affects the conformation of the linker between the large and small AAA+ domains and changes the rotation between these domains. These movements propagate around the ring, resulting in a flexing motion in which some structural elements move down while others move up relative to the pore axis.

Additional conformations, for example those stabilized by ATP and substrate binding, will certainly be utilized during ClpX function. We anticipate, however, that the structural principles noted above will still apply. Specifically, we expect that ATP binding, hydrolysis to ADP•P_i, and release of P_i and/or ADP during the ATPase cycle will alter the rotation between the large and small AAA+ domains of the subunit in which the reaction occurs. These changes will cause rigid-body conformational changes throughout the ClpX hexamer, which can be coupled to mechanical work on protein and polypeptide substrates.

Our structures lack the ClpX N domain, which forms a dimer and serves as a tethering site for adaptor proteins and certain substrates (Singh et al., 2001; Wojtyra et al., 2003; Donaldson et al., 2003; Park et al., 2007). In intact ClpX, a 15-residue linker connects each N domain to the large AAA+ domain. We found that three N-domain dimers could be modeled near the periphery of the hexameric ring, without steric clashes and with linking distances to the appropriate large AAA+ domains of roughly 20 Å (Fig. 5C). Because an extended 15-residue linker could span up to 40 Å, each N-domain dimer should be somewhat flexible in the ClpX hexamer.

An IGF sequence in ClpX makes important docking contacts with hydrophobic clefts on the surface of the ClpP ring (Wang et al., 1997; Kim et al., 2001; Singh et al., 2001; Martin et al., 2007). We did not attempt to model this interaction because the ClpX IGF loops (residues 261-284) were almost completely disordered in our structures and there is no simple match between the symmetric ClpP heptamer and the asymmetric ClpX hexamer.

Functional consequences of pore-loop staggering

The loops that form the axial pore of ClpX are involved in recognition of the ssrA-degradation tag, binding and communicating with ClpP, and substrate unfolding and translocation. The basic RKH loops surround the pore entry and interact favorably with the negatively charged α-carboxylate of the ssrA tag, apparently stabilizing an encounter complex before the tag moves deeper into the pore to interact with the GYVG and pore-2 loops (Farrell et al., 2007; Martin et al., 2008a). Although the RKH loops are disordered in our structures, the positions from which they project from the hexamer are axially staggered. This arrangement provides a path to guide the ssrA tag into the lumen of the pore, where the GYVG and pore-2 loops could then engage the substrate to facilitate unfolding and translocation.

Axial staggering can explain why the pore-2 loops can crosslink to the N-terminal loops of ClpP, which contact ClpX near the bottom of the axial pore, and also to the SspB adaptor protein, which can only enter the top portion of the pore (Martin et al., 2007; 2008a). These results would be extremely difficult to understand if the ClpX hexamer had approximate six-fold symmetry, because all pore-2 loops would occupy similar axial positions. In our nucleotide-bound hexamer, however, the pore-2 loops of the type-2 subunits are close to the top of the pore, where they could easily crosslink to SspB, whereas those of the type-1 subunits are close to the bottom face of the hexamer, where ClpP binds (Fig. 5B). Interactions with ClpP, mediated by the pore-2 loops, regulate the ATPase rate of wild-type ClpX (Martin et al., 2007). Thus, it seems probable that the pore-2 loops of type-1 subunits interact with ClpP in a fashion that alters the rate of ATP-hydrolysis in these subunits. The Walker-B motif, which contacts ATP and participates in catalysis, immediately precedes the pore-2 loop in the ClpX sequence, and thus even small ClpP-mediated variations in the conformation of these loops might be propagated to the active site.

Both the GYVG loops and the pore-2 loops are required for strong binding to the ssrA tag and for robust protein unfolding (Siddiqui et al., 2004; Martin et al., 2008a; 2008b). Axial staggering places the GYVG loops of some subunits next to the pore-2 loops of other subunits, and it is plausible that a binding site for the ssrA tag is formed by an interaction between both loops. The importance of the GYVG and pore-2 loops in protein unfolding could be explained by roles in translocation and/or in preventing substrate slipping following translocation. Mutations in the GYVG loops but not the pore-2 loops slow translocation, and thus the pore-2 loops may function largely to grip substrates after a translocation step. In this regard, the four pore-2 loops of type-1 subunits are close to one another and encircle a narrow channel near the bottom of the pore. Thus, a polypeptide substrate could potentially be pinned in this channel, while the enzyme resets for the next translocation step.

Among the three types of ClpX pore loops, only the GYVG loops are highly conserved in other AAA+ proteases (Wang et al., 2001; Siddiqui et al., 2004). Thus, these loops are thought to play the major role in substrate translocation and protein unfolding by ClpX. Genetic and biochemical studies support this model and show that the GYVG loops play important roles in gripping the polypeptide substrate (Martin et al., 2008b). Because the GYVG loops occupy different axial positions in our structures, it is plausible that ATP binding and/or hydrolysis could cause a given GYVG loop to move downward in the pore as a consequence of the rigid-body movement of the large AAA+ domain in which it resides. For example, Tyr153 in the GYVG loop of chain E moves down through the pore upon nucleotide binding, and similar loop motions during the ATPase cycle could pull or drag a bound polypeptide substrate along, providing a mechanism for translocation and force application (Fig. 6A).

A mechanism for pore elasticity

ClpX translocates polyglycine sequences efficiently but must also translocate three polypeptides together when it degrades disulfide-bonded proteins (Burton *et al.*, 2001; Bolon et al., 2004; Barkow et al., 2009). However, the GYVG and pore-2 loops fill most of the space in the pore, and it appears unlikely that even a single translocating polypeptide with bulky side chains could fit without some structural rearrangements (Fig. 1D). Our structures, however, suggest a mechanism by which the pore could expand to accommodate substrates of increasing size. If we think of the axial pore as a mouth, then the hexameric ring has two jaws, connected largely by a hinge-like linker between the large and small AAA+ domains of each type-2 subunit, (Fig. 6B; see also Fig. 4C). We propose that one or both of these hinge interfaces open in an elastic fashion, to allow passage of substrates that are too large to transit the undistorted pore (Fig. 6B). Opening might occur by unraveling the type-2 linker (or part of the adjacent 320-327 helix) as a consequence of attempts by ClpX to force translocation of larger substrates.

Refolding, in the absence of any force, could reclose the pore. This model is analogous to the elastically hinged jaws of a snake, which allow it to consume prey larger than its normal mouth size. The inability of type-2 subunits to bind nucleotide is an important aspect of our pore-expansion model, because ligand binding at the "hinge" interface would hinder opening. A reasonably constricted pore in the absence of distorting forces is another requisite feature, because the enzyme needs to maintain close contacts with skeletal substrates consisting of little more than the polypeptide backbone both to drive translocation of such substrates and to prevent substrate slipping/dissociation between power strokes.

Comparison with other AAA+ hexamers

In crystals, AAA+ hexamers have been found to be 6-fold symmetric, to form dimer-of-trimers or trimer-of-dimers rings, to have a screw axis relating adjacent subunits, or to lack symmetry entirely (Bochtler et al., 2000; Singleton et al., 2000; Sousa et al., 2000; 2002; Wang et al., 2001; Kwon et al., 2003; Gai et al., 2004; Bieniossek *et al.*, 2006; Enemark and Joshua-Tor, 2006; Skordalakes and Berger, 2006). Because most of these AAA+ machines perform vectorial work on polypeptide or nucleic-acid substrates, which themselves lack symmetry, it would be reasonable if the functional solution conformations of these enzymes were also asymmetric. The crystallographic ClpX rings most closely resembled dimers of trimers, but both hexamers were fundamentally asymmetric. Indeed, because ClpX appears to operate by a stochastic mechanism in which only one ATP is hydrolyzed per power stroke (Martin et al., 2005), asymmetry is a natural consequence of function.

Like ClpX, several AAA+ hexamers crystallize with four nucleotide-bound and two nucleotide-free subunits (Bochtler et al., 2000; Singleton et al., 2000). However, the unoccupied subunits in these hexamers differ modestly in structure from the nucleotide-bound subunits. By contrast, the type-2 subunits in ClpX differ radically different from the type-1 nucleotide-binding subunits, as a consequence of differences in rotation approaching 80° between the two AAA+ domains (Fig. 1F, 3C). These very large changes in domain-domain orientation result in the dramatic staggering of domains and structural elements around the ClpX ring. By contrast, rotations between the large and small AAA+ domains of different subunits in hexamers of HslU and FtsH (other proteolytic AAA+ enzymes) do not exceed 15° and result in only minor deviations from planar hexamers. Indeed, attempts to model a wide variety of AAA+ ring hexamers from monomeric subunits have used the relative orientation of the large and small AAA+ domains as a tight constraint (Diemand and Lupas, 2006), limiting models to a much narrower range of domain-domain rotations than we observe in ClpX.

The type-1 and type-2 subunits of ClpX clearly play different structural and functional roles in the hexameric ring. It is possible that type-1 and type-2 subunits undergo some type of coordinated interconversion during each ATP-fueled power stroke. If this were the case, then additional arrangements of type-1 and type-2 subunits in the ring (e.g., 1-1-2-1-2-1, 1-1-2-2-1-1, etc.) might be expected to exist. Alternatively, two ClpX subunits might simply adopt and maintain the type-2 role throughout a complete proteolytic cycle of unfolding and translocation. In this instance, only the dedicated type-1 subunits would cycle through different nucleotide states, although these states could alter the conformation of the entire ring. In either case, ClpX appears to represent an interesting transition between homomeric AAA+ machines in which all subunits adopt similar structures, even if they function as asymmetric multimers, and heteromeric machines (dynein, Mcm2-7 helicase, the proteasome, etc.) in which each AAA + subunit/module in the ring has evolved to have a different sequence and function.

Structure and function

The rotation between the large and small AAA+ domains in the type-2 subunits of the ClpX structures appears to be without precedent in related homomeric AAA+ machines, and one

might worry that it represents an artifact of crystallization, the E185Q/R370K mutations, or the tethering linkers used to connect subunits. With respect to crystal contacts, we note that the basic architecture was maintained in two crystal lattices. The 20-residue tethering linkers were unstructured, and thus it is difficult to imagine that they dictate the structures observed. Moreover, ClpX subunits connected by these tethers are as active as wild type (Martin et al., 2005). Indeed, our structures suggested that these tethers could be roughly half as long and still connect adjacent subunits without strain. When we constructed a ClpX-ΔN variant with an 11-residue tether, it had degradation and ATPase activities indistinguishable from the parental enzyme with the 20-residue tether (Supplementary Figs. 1 and 2). With respect to mutations, single-chain ClpX with E185Q or R370K substitutions in four subunits function as efficient unfoldases and translocases (Martin et al., 2005), making it very unlikely that these conservative side-chain substitutions distort the structure. Finally, a partially refined structure in which subunits were tethered but lacked the E185Q/R370K mutations revealed the same basic arrangement of subunits seen in the structures presented here (unpublished). This "wild-type" structure has been refined to 3.8 Å resolution (current statistics, R=0.31, R_{free}=0.33) by the same methods used for the mutant structures and shows a clear 1-1-2-1-1-2 subunit pattern.

The strongest argument for relevance of our structures is that they are consistent with and provide a structural rationale for a large body of experiments. For example, the presence of two type-2 subunits in our structures explains why ClpX homohexamers bind no more than four ATP molecules, and structural differences among nucleotide-bound type-1 subunits explain the existence of multiple kinetic classes of bound ATP molecules (Hersch et al., 2005). Similarly, the axial staggering of pore loops in the hexamer explains mutational and crosslinking studies of the interaction of ClpX with the ssrA tag, with the SspB adaptor, and with ClpP (Martin et al. 2007; 2008a; 2008b). Structural asymmetry is consistent with the finding that covalently linked ClpX variants with only a subset of subunits capable of hydrolyzing ATP still unfold and translocate protein substrates efficiently (Martin et al., 2005). Moreover, mutations in the rigid-body interface between the small AAA+ domain and the neighboring large AAA+ domain alter ClpX's ability to unfold native substrates and disassemble macromolecular complexes (Joshi et al., 2003; 2004), consistent with our structure-based proposal that these interfaces transmit conformational changes initiated in one nucleotide-binding site to the rest of the ring. Finally, our structures suggest a pore expansion/contraction mechanism that explains ClpX's ability to translocate diverse substrates, ranging in size and polypeptide number. We anticipate that the structures presented here will provide a foundation for future studies aimed at probing the detailed mechanisms by which ATP binding, ATP hydrolysis, and ADP/Pi release are coupled to mechanical work during the operation of ClpX and related AAA+ machines.

Experimental Procedures

Protein expression and purification

The ClpX variant used for crystallization contained three *E. coli* ClpX-ΔN subunits (residues 61-423) connected by linkers with the sequence ASGAGGSEGGGSEGGTSGAT and contained an N-terminal H_6 tag (Martin et al., 2005). In addition, each subunit contained an E185Q mutation and the C-terminal subunit contained an additional R370K mutation. This protein was expressed in *E. coli* BLR (DE3) cells and was purified as described (Martin *et al.*, 2007). The protein was concentrated to a final concentration of 40 μM in 50 mM Tris-HCl (pH 7.5), 300 mM KCl, 10% glycerol, 0.1 mM EDTA, and 1 mM DTT.

Crystallization and data collection

Nucleotide-free ClpX crystals were grown using the hanging-drop method of vapor diffusion. Well solution (1 μL) containing 1.9 M ammonium sulfate and 75 mM sodium acetate (pH 4.8)

was mixed with 1 μL of protein solution and incubated at room temperature for approximately 12 weeks. Crystals of nucleotide-bound ClpX were produced by soaking a nucleotide-free crystal in a solution containing the crystal mother liquor plus 5 mM ATPγS (Calbiochem) and 5 mM MgCl$_2$ for approximately 12 hrs. Crystals were cryo-protected by coating in Paratone-N (Hampton Research) and immediately flash cooled in liquid nitrogen prior to being screened for X-ray diffraction. X-ray diffraction data were collected at the 24-ID-C beamline of the Advanced Photon Source, Argonne National Laboratories (Argonne, IL) using a Quantum 315 detector. Nucleotide-free ClpX data were collected with a crystal to detector distance of 400 mm, an oscillation of 1°, and an exposure time of 2 s. Crystals belonged to space group P2$_1$2$_1$2$_1$, with unit cell dimensions of a = 63.3 Å, b = 199.9 Å, c = 202.5 Å, α=β=γ=90° and diffracted to 4.0 Å resolution. Consideration of the unit-cell volume indicated the presence of two ClpX pseudo-trimers in the asymmetric unit (Matthews, 1977). Data from nucleotide-soaked ClpX crystals were collected with a crystal to detector distance of 450 mm, an oscillation of 0.5°, and an exposure time of 2 s. Soaked crystals had a significantly smaller unit cell, with dimensions a = 54.1 Å, b = 178.5 Å, c = 201.4 Å and diffracted to 3.25 Å resolution.

Data processing, structure solution, and refinement

Diffraction data were integrated and scaled using HKL2000 (Otwinowski and Minor, 1997) and converted to structure-factor amplitudes using TRUNCATE (CCP4, 1994). Final data processing statistics are shown in Table 1. The structure of an *H. pylori* ClpX subunit (Kim and Kim, 2003) was used as a search model in a combination of automated molecular replacement with PHASER (McCoy et al., 2007) and manual real space fitting in COOT (Emsley and Cowtan, 2004). The initial model underwent iterative rounds of model building in COOT and rigid-body and group-ADP refinement in PHENIX (Adams et al., 2002); individual large and small AAA+ domains were defined as rigid-body groups with a single temperature factor. Improved electron-density maps were produced after each round of model refinement through non-crystallographic symmetry averaging in DM (CCP4, 1994) with the core of the two domains averaged independently, and B-factor sharpening in CNSsolve1.2 (Brunger et al., 1998). Examination of mFo-DFc maps calculated on a refined nucleotide-free ClpX model revealed the presence of strong peaks of positive density in the 'nucleotide-binding' sites of each subunit, which were built as sulfate ions. Similar maps calculated on a refined model of nucleotide-soaked ClpX showed the presence of strong density corresponding to bound nucleotide in chains A, B, and E. Chain D had weaker nucleotide density. After convergence of the refinement, final cycles of individual atom positional refinement were performed using tight NCS restraints and one B-factor per residue. The position of each domain in the final structure was confirmed using simulated-annealing omit maps calculated in PHENIX (Adams et al., 2002).

Structure analysis

Rotation angles between the large and small AAA+ domains of each ClpX subunit and other AAA+ ATPases were calculated using the DynDom program (Hayward and Berendsen, 1998). Superposition of structures was carried out using LSKQAB (CCP4, 1994) and buried surface areas were calculated using the PISA server (Krissinel and Henrick, 2007; http://www.ebi.ac.uk/msd-srv/prot_int/pistart.html). Figures were prepared using PyMOL (DeLano, 2002). Morphs for the ClpX motion movie were produced by the Yale Morph Server (Krebs and Gerstein, 2000; http://www2.molmovdb.org/wiki/info/index.php/Morph_Server) and were displayed, animated, and rendered in PYMOL (DeLano, 2002).

Supplementary Material

Refer to Web version on PubMed Central for supplementary material.

Acknowledgments

References

Adams PD, Grosse-Kunstleve RW, Hung LW, Ioerger TR, McCoy AJ, Moriarty NW, Read RJ, Sacchettini JC, Sauter NK, Terwilliger TC. PHENIX: building new software for automated crystallographic structure determination. Acta Cryst. Sect. D 2002;58:1948–1954. [PubMed: 12393927]

Barkow S, Levchenko I, Baker TA, Sauer RT. Polypeptide translocation by the AAA+ ClpXP protease machine. Chem. Biol 2009;16:605–612. [PubMed: 19549599]

Bieniossek C, Schalch T, Bumann M, Meister M, Meier R, Baumann U. The molecular architecture of the metalloprotease FtsH. Proc. Natl. Acad. Sci. USA 2006;103:3066–3071. [PubMed: 16484367]

Bochtler M, Hartmann C, Song HK, Bourenkov GP, Bartunik HD, Huber R. The structures of HslU and the ATP-dependent protease HslU-HsIV. Nature 2000;403:800–805. [PubMed: 10693812]

Bolon DN, Grant RA, Baker TA, Sauer RT. Nucleotide-dependent substrate handoff from the SspB adaptor to the AAA+ ClpXP protease. Mol. Cell 2004;16:343–350. [PubMed: 15525508]

Brunger AT, Adams PD, Clore GM, Delano WL, Gros P, Gross-Kunstleve RW, Jiang J-S, Kuszewski J, Nilges N, Pannu NS, Read RJ, Rice LM, Simonson T, Warren GL. Crystallography and NMR system (CNS): A new software system. Acta Crystallog. D 1998;54:905–921.

Burton RE, Siddiqui SM, Kim YI, Baker TA, Sauer RT. Effects of protein stability and structure on substrate processing by the ClpXP unfolding and degradation machine. EMBO J 2001;20:3092–3100. [PubMed: 11406586]

Collaborative Computing Project 4 (CCP4). The CCP4 suite: programs for protein crystallography. Acta Crystallog. D 1994;50:760–763.

DeLano, WL. 2002. http://www.pymol.org

Diemand AV, Lupas AN. Modeling AAA+ ring complexes from monomeric structures. J. Struc. Biol 2006;156:230–243.

Donaldson LW, Wojtyra U, Houry WA. Solution structure of the dimeric zinc binding domain of the chaperone ClpX. J. Biol. Chem 2003;278:48991–48996. [PubMed: 14525985]

Emsley P, Cowtan K. Coot: model-building tools for molecular graphics. Acta Cryst. Sect. D 2004;60:2126–2132. [PubMed: 15572765]

Enemark EJ, Joshua-Tor L. Mechanism of DNA translocation in a replicative hexameric helicase. Nature 2006;442:270–275. [PubMed: 16855583]

Erzberger JM, Berger JP. Evolutionary relationships and structural mechanisms of AAA+ proteins. Annu. Rev. Biophys. Biomol. Struct 2006;35:93–114. [PubMed: 16689629]

Farrell CM, Baker TA, Sauer RT. Altered specificity of a AAA+ protease. Mol. Cell 2007;25:161–166. [PubMed: 17218279]

Gai D, Zhao R, Li D, Finkielstein CV, Chen XS. Mechanisms of conformational change for a replicative hexameric helicase of SV40 large tumor antigen. Cell 2004;119:47–60. [PubMed: 15454080]

Gottesman S, Roche E, Zhou Y, Sauer RT. The ClpXP and ClpAP proteases degrade proteins with carboxy-terminal peptide tails added by the SsrA-tagging system. Genes Dev 1998;12:1338–1347. [PubMed: 9573050]

Grimaud R, Kessel M, Beuron F, Steven AC, Maurizi MR. Enzymatic and structural similarities between the Escherichia coli ATP-dependent proteases, ClpXP and ClpAP. J. Biol. Chem 1998;273:12476–12481. [PubMed: 9575205]

Hanson PI, Whiteheart SW. AAA+ proteins: have engines, will work. Nat. Rev. Mol. Cell. Biol 2005;6:519–529. [PubMed: 16072036]

Hayward S, Berendsen HJC. Systematic analysis of domain motions in proteins from conformational change: New results on citrate synthase and T4 lysozyme. Proteins-Structure, Function and Genetics 1998;30:144–154.

Hersch GL, Burton RE, Bolon DN, Baker TA, Sauer RT. Asymmetric interactions of ATP with the AAA + ClpX6 unfoldase: allosteric control of a protein machine. Cell 2005;121:1017–1027. [PubMed: 15989952]

Joshi SA, Baker TA, Sauer RT. C-terminal domain mutations in ClpX uncouple substrate binding from an engagement step required for unfolding. Mol. Micro 2003;48:67–76.

Joshi SL, Hersch GL, Baker TA, Sauer RT. Communication between ClpX and ClpP during substrate processing and degradation. Nat. Struct. Mol. Biol 2004;11:404–411. [PubMed: 15064753]

Kim YI, Levchenko I, Fraczkowska K, Woodruff RV, Sauer RT, Baker TA. Molecular Determinants of Complex Formation between Clp/Hsp100 ATPases and the ClpP Peptidase. Nat. Struct. Biol 2001;8:230–233. [PubMed: 11224567]

Kim DY, Kim KK. Crystal structure of ClpX molecular chaperone from *Helicobacter pylori*. J. Biol Chem 2003;278:50664–50670. [PubMed: 14514695]

Kim YI, Burton RE, Burton BM, Sauer RT, Baker TA. Dynamics of substrate denaturation and translocation by the ClpXP degradation machine. Mol. Cell 2000;5:639–648. [PubMed: 10882100]

Krebs WG, Gerstein M. The morph server: a standardized system for analyzing and visualizing macromolecular motions in a database framework. Nuc. Acids Res 2000;28:1665–1675.

Krissinel E, Henrick K. Inference of macromolecular assemblies from crystalline state. J. Mol. Biol 2007;372:774–797. [PubMed: 17681537]

Kwon AR, Kessler BM, Overkleeft HS, McKay DB. Structure and reactivity of an asymmetric complex between HslV and I-domain deleted HslU, a prokaryotic homolog of the eukaryotic proteasome. J. Mol. Biol 2003;330:185–195. [PubMed: 12823960]

Levchenko I, Yamauchi M, Baker TA. ClpX and MuB interact with overlapping regions of Mu transposase: implications for control of the transposition pathway. Genes Dev 1997;11:1561–1572. [PubMed: 9203582]

Martin A, Baker TA, Sauer RT. Rebuilt AAA + motors reveal operating principles for ATP-fuelled machines. Nature 2005;437:1115–1120. [PubMed: 16237435]

Martin A, Baker TA, Sauer RT. Distinct static and dynamic interactions control ATPase-peptidase communication in a AAA+ protease. Mol. Cell 2007;27:41–52. [PubMed: 17612489]

Martin A, Baker TA, Sauer RT. Diverse pore loops of the AAA+ ClpX machine mediate unassisted and adaptor-dependent recognition of ssrA-tagged substrates. Mol. Cell 2008a;29:441–450. [PubMed: 18313382]

Martin A, Baker TA, Sauer RT. Pore loops of the AAA+ ClpX machine grip substrates to drive translocation and unfolding. Nat. Struct. Mol. Biol 2008b;15:1147–1151. [PubMed: 18931677]

Matthews BW. Solvent content of crystals. J. Mol. Biol 1968;33:491–497. [PubMed: 5700707]

McCoy AJ, Grosse-Kunstleve RW, Adams PD, Winn MD, Storoni LC, Read RJ. Phaser crystallographic software. J. Appl. Cryst 2007;40:658–674. [PubMed: 19461840]

Ortega J, Singh SK, Ishikawa T, Maurizi MR, Steven AC. Visualization of substrate binding and translocation by the ATP-dependent protease, ClpXP. Mol. Cell 2000;6:1515–1521. [PubMed: 11163224]

Otwinowski Z, Minor W. Processing of X-ray Diffraction Data Collected in Oscillation Mode. Methods Enz 1997;276:307–326.

Park EY, Lee BG, Hong SB, Kim HW, Jeon H, Song HK. Structural basis of SspB-tail recognition by the zinc binding domain of ClpX. J. Mol. Biol 2007;367:514–526. [PubMed: 17258768]

Schirmer EC, Glover JR, Singer MA, Lindquist S. HSP100/Clp proteins: a common mechanism explains diverse functions. Trends Biochem Sci 1996;21:289–296. [PubMed: 8772382]

Siddiqui SM, Sauer RT, Baker TA. Role of the processing pore of the ClpX AAA+ ATPase in the recognition and engagement of specific protein substrates. Genes Dev 2004;18:369–374. [PubMed: 15004005]

Singh SK, Grimaud R, Hoskins JR, Wickner S, Maurizi MR. Unfolding and internalization of proteins by the ATP-dependent proteases ClpXP and ClpAP. Proc. Natl. Acad. Sci. USA 2000;97:8898–8903. [PubMed: 10922052]

Singh SK, Rozycki J, Ortega J, Ishikawa T, Lo J, Steven AC, Maurizi MR. Functional domains of the ClpA and ClpX molecular chaperones identified by limited proteolysis and deletion analysis. J. Biol. Chem 2001;276:29420–29429. [PubMed: 11346657]

Singleton MR, Sawaya MR, Ellenberger T, Wigley DB. Crystal structure of T7 gene 4 ring helicase indicates a mechanism for sequential hydrolysis of nucleotides. Cell 2000;101:589–600. [PubMed: 10892646]

Skordalakes E, Berger JM. Structural insights into RNA-dependent ring closure and ATPase activation by the Rho termination factor. Cell 2006;127:553–564. [PubMed: 17081977]

Sousa MC, Trame CB, Tsuruta H, Wilbanks SM, Reddy VS, McKay DB. Crystal and solution structures of an HslUV protease-chaperone complex. Cell 2000;103:633–643. [PubMed: 11106733]

Sousa MC, Kessler BM, Overkleeft HS, McKay DB. Crystal structure of HslUV complexed with a vinyl sulfone inhibitor: corroboration of a proposed mechanism of allosteric activation of HslV by HslU. J. Mol. Biol 2002;318:779–785. [PubMed: 12054822]

Tucker PA, Sallai L. The AAA+ superfamily: a myriad of motions. Curr. Opin. Struct. Biol 2007;17:641–652. [PubMed: 18023171]

Wang J, Hartling JA, Flanagan JM. The structure of ClpP at 2.3 Å resolution suggests a model for ATP-dependent proteolysis. Cell 1997;91:447–456. [PubMed: 9390554]

Wang J, Song JJ, Franklin MC, Kamtekar S, Im YJ, Rho SH, Seong IS, Lee CS, Chung CH, Eom SH. Crystal structures of the HslVU peptidase-ATPase complex reveal an ATP-dependent proteolysis mechanism. Structure 2001;9:177–184. [PubMed: 11250202]

White SR, Lauring B. AAA+ ATPases: achieving diversity of function with conserved machinery. Traffic 2007;8:1657–1667. [PubMed: 17897320]

Wojtyra UA, Thibault G, Tuite A, Houry WA. The N-terminal zinc binding domain of ClpX is a dimerization domain that modulates the chaperone function. J. Biol. Chem 2003;278:48981–48990. [PubMed: 12937164]

Yakamavich JA, Baker TA, Sauer RT. Asymmetric nucleotide transactions of the HslUV protease. J. Mol. Biol 2008;380:946–57. [PubMed: 18582897]
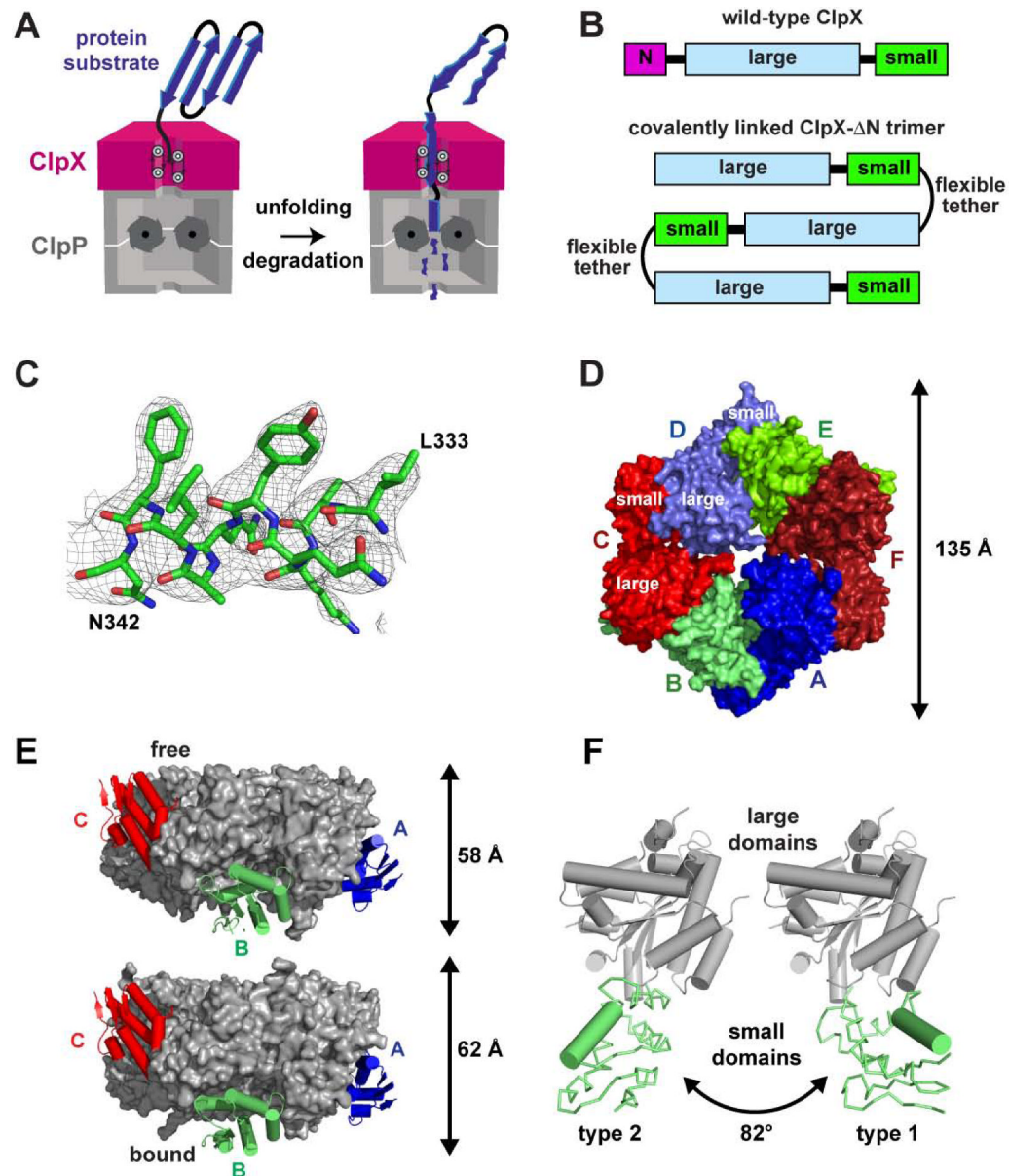
Figure 1. Asymmetric Structures of ClpX Hexamers

(**A**) Model for protein unfolding and degradation by the ClpXP protease. Cutaway view showing how the degradation tag of a protein substrate could initially bind in the pore of ClpX. ATP-dependent translocation could then lead to unfolding and degradation of the polypeptide by ClpP.

(**B**) Domain structures of wild-type ClpX and the covalently linked ClpX-ΔN trimer.

(**C**) Portion of the refined $2F_O$-F_c electron-density map (contoured at 1σ) for the nucleotide-bound hexamer.

(**D**) Surface representation of the nucleotide-bound ClpX hexamer, viewed from the top or ClpP-distal face. Each subunit is a different color. The large and small AAA+ domains of two adjacent subunits are labeled.

(**E**) Side views of the nucleotide-free (top) and nucleotide-bound (bottom) hexamers in mixed surface/cartoon representation. The staggered positions of the small AAA+ domains in chain A (blue), in chain B (green), and in chain C (red) are shown.

(F) The large AAA+ domains of a type-1 subunit (chain A) and type-2 subunit (chain C) from the nucleotide-bound hexamer are shown in the same orientation, revealing a large change in the relative orientation of the attached small AAA+ domains. In the small domains, only the helix formed by residues 333-344 is shown in cartoon representation.
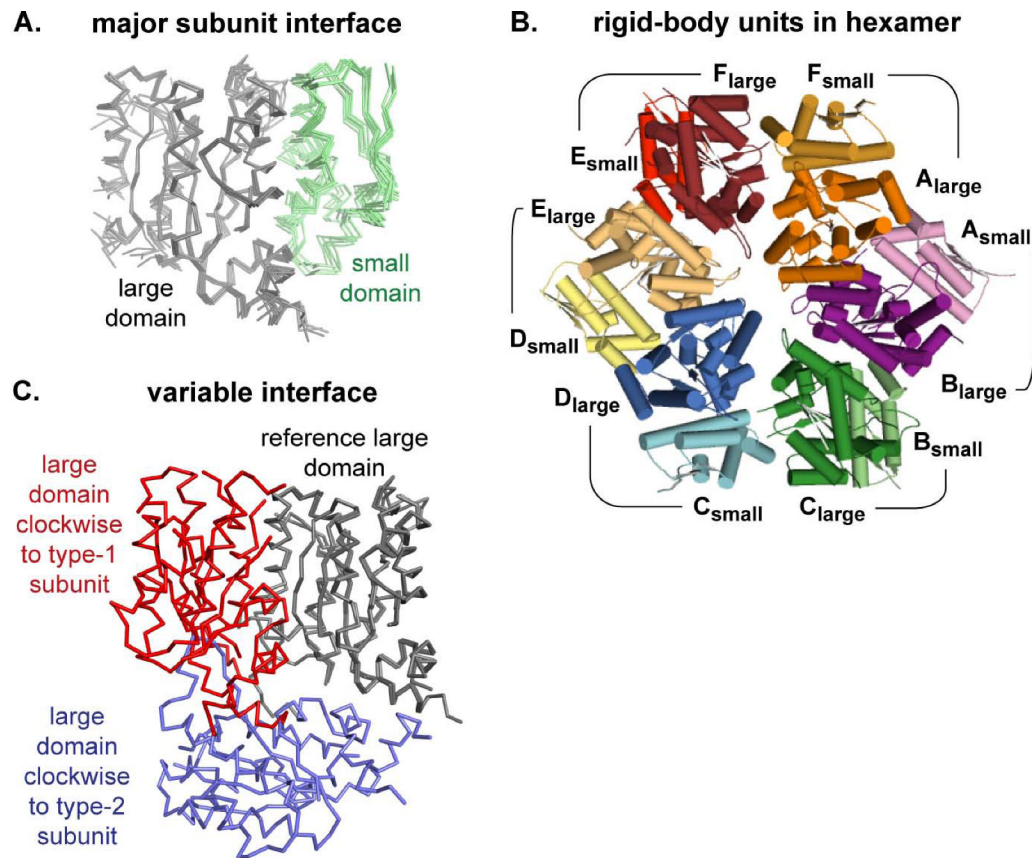
Figure 2. Subunit-Subunit Interfaces

(A) The large AAA+ domains (grey; Cα trace) from all six subunits of the nucleotide-bound hexamer were superimposed, showing highly conserved positions of the small AAA+ domain (green) in the counter-clockwise subunit. The same orientation of adjacent large and small AAA+ domains was seen in nucleotide-free ClpX, suggesting that these neighboring domains comprise a rigid-body unit.

(B) The six rigid-body units in the nucleotide-bound ClpX hexamer (top view; cartoon representation) are shown in different colors, with the small AAA+ domain of each rigid-body unit colored a lighter shade (e.g., A_{small}; light purple) than the clockwise large AAA+ domain in the same unit (e.g., B_{large}; dark purple).

(C) Modules consisting of two adjacent large AAA+ domains from the nucleotide-bound hexamer were compared by superimposing the B domain of the B/C module on the C domain of the C/D module. This alignment shows that a large AAA+ domain clockwise from a type-1 subunit (red) occupies a very different position from a large AAA+ domain clockwise to a type-2 subunit (blue).
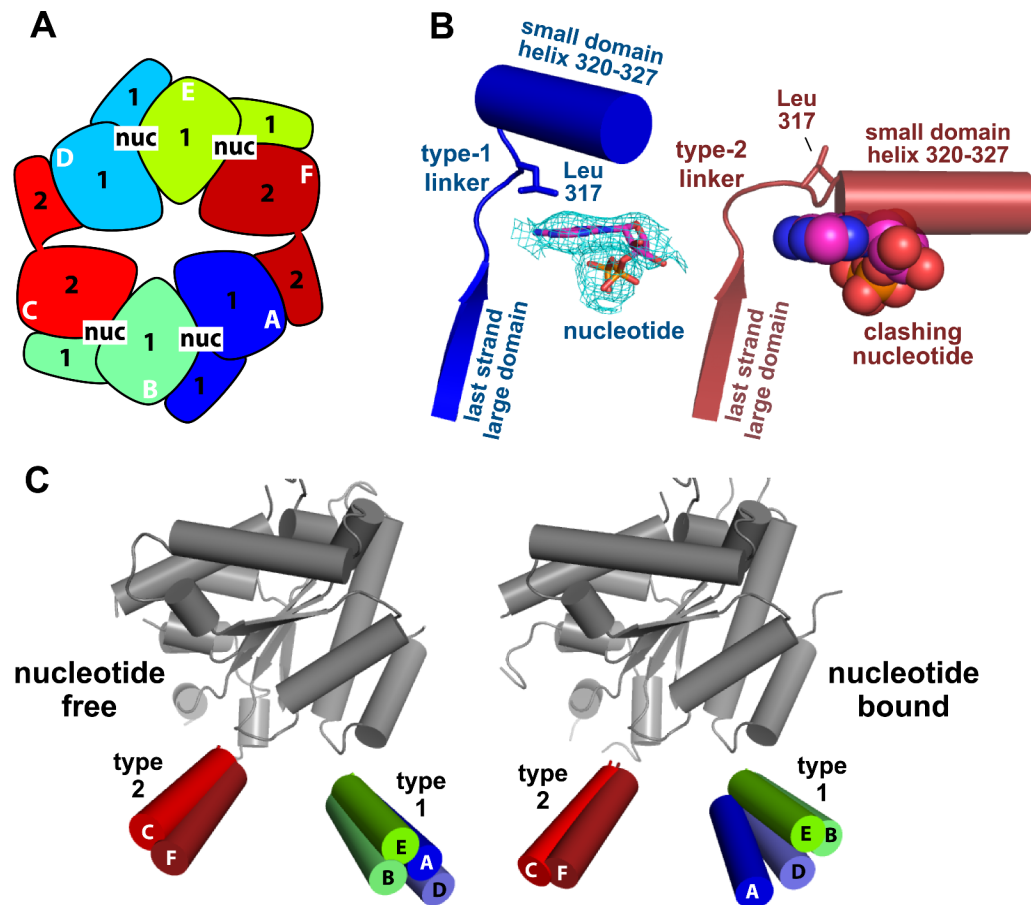
Figure 3. Nucleotide Binding

(**A**) Cartoon of the nucleotide-bound ClpX hexamer showing the positions of the four nucleotide-binding sites relative to type-1 and type-2 subunits.

(**B**) Mixed cartoon/stick representation of the inter-domain linkers from a type-1 subunit (chain A, blue) and type-2 subunit (chain F, dark red) from the nucleotide-bound structure. In the type-1 subunit, the side chain of Leu317 contacts the adenine base of the nucleotide (modeled as ADP in stick representation; $2F_o$-F_c electron density contoured at 1σ). The linker in the type-2 subunit has a completely different conformation; Leu317 points in the opposite direction, and helix 320-327 of the small AAA+ domain clashes with modeled nucleotide.

(**C**) The large AAA+ domains of each subunit (gray) in the nucleotide-free and nucleotide-bound hexamers were aligned, showing that nucleotide binding changes the rotation of some small AAA+ domains (represented by a single colored α-helix formed by residues 333-344) relative to the large domain.
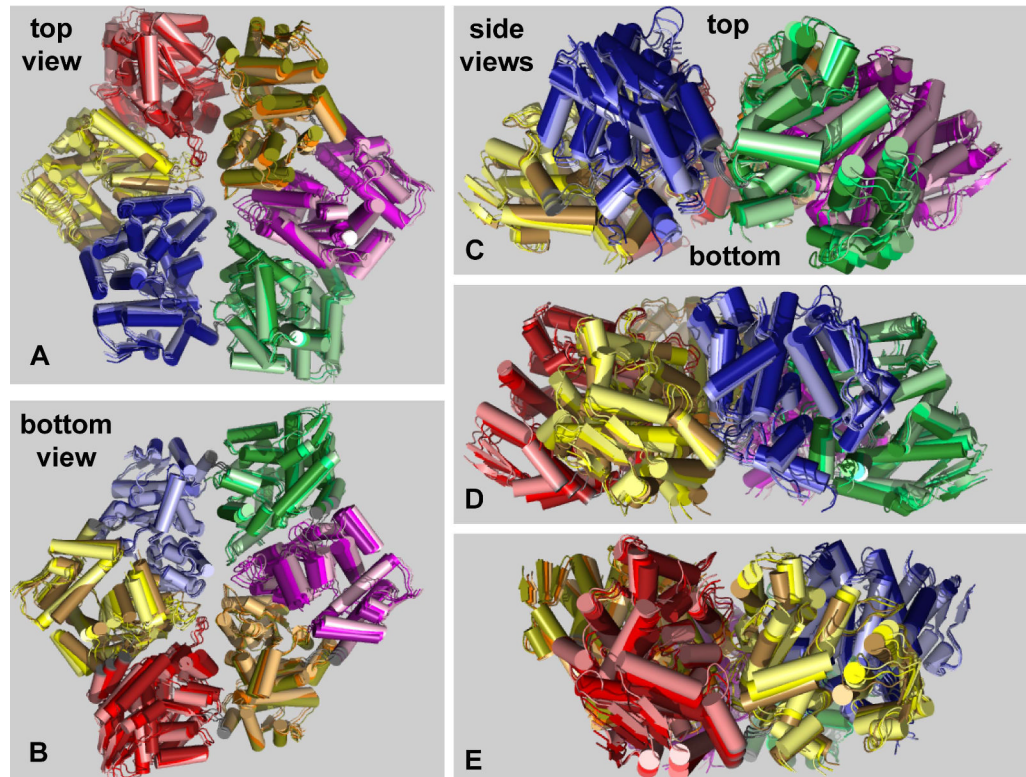
Figure 4. Nucleotide-Dependent Motions
(A) Top, **(B)** bottom, and side views **(C-E)** of the nucleotide-free and nucleotide-bound ClpX hexamers in cartoon representation following superposition. An intermediate structure obtained by averaging is also shown. For each structure, each of the six rigid-body units is a different color. Within each unit, lighter shades represent the nucleotide-free structure, intermediate shades represent the averaged structure, and darker shades represent the nucleotide-bound structure. Thus, motions induced by nucleotide binding progress from lighter to darker shades. Asymmetry of the nucleotide-free and nucleotide-bound hexamers is evident in the top and bottom views (looking along the axis of the pore) and in the side views. The views in panel B and C were generated from that in panel A by 180° and 90° rotations, respectively, around the x-axis. The views shown in panels D and E represent rotations around the y-axis in 50° and 75° increments from the view in panel C.
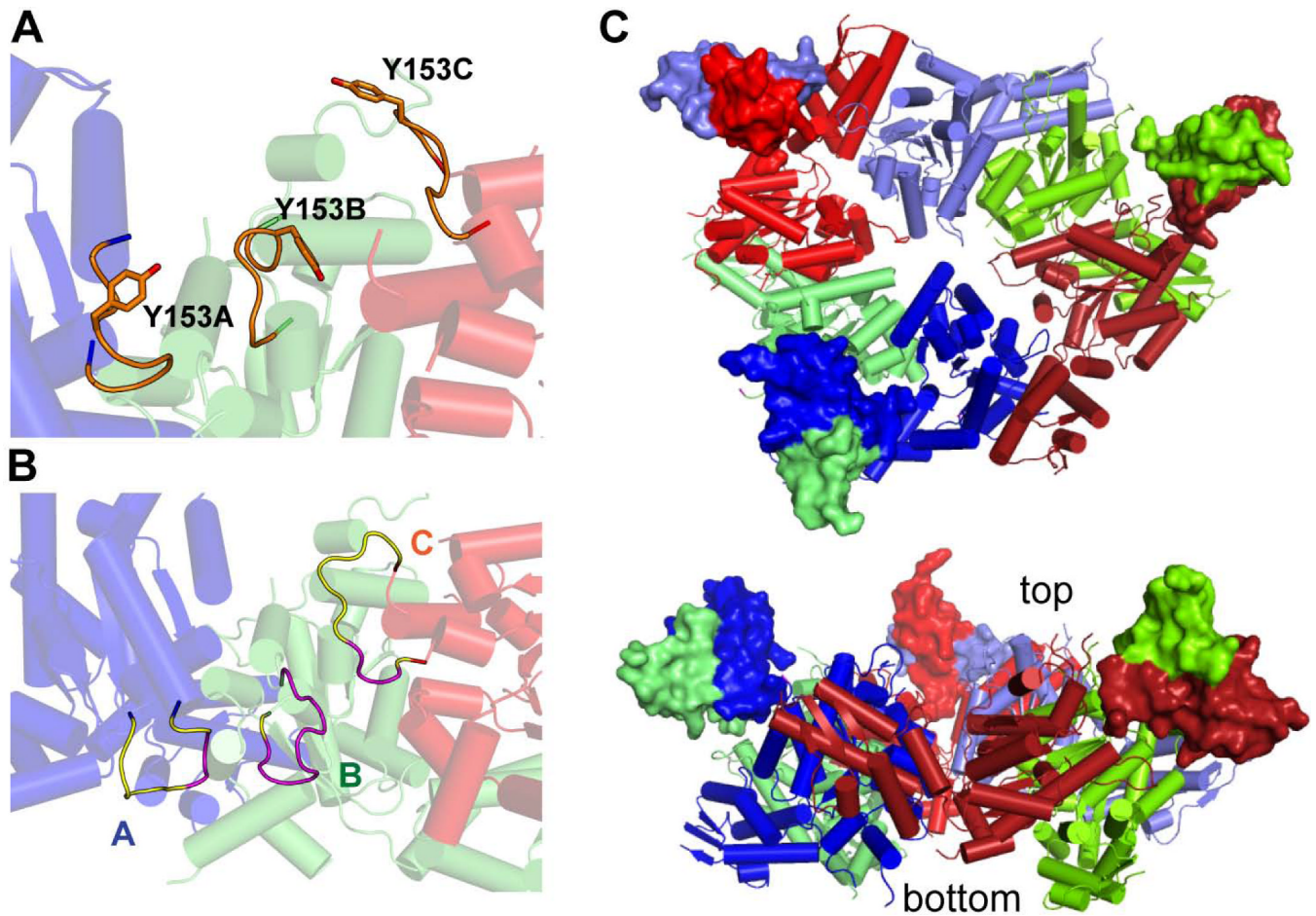
Figure 5. Positions of Pore Loops and Modeled N-domains

(**A**) Cartoon representation of the GYVG loops (orange) from subunits A (blue), B (green) and C (red) of the nucleotide-bound ClpX hexamer viewed perpendicular to the axial pore, which runs from the top to the bottom. Tyr153 is shown in stick representation.

(**B**) Cartoon of the pore-2 loops (structured parts yellow; modeled parts purple) from subunits A (blue), B (green) and C (red) of the nucleotide-bound ClpX hexamer. Same orientation as panel A.

(**C**) Models showing two views of how three N-domain dimers of ClpX (surface representation; Donaldson et al., 2003; Park et al., 2007) could connect to the nucleotide-bound hexamer (cartoon representation). Although explicit linkers were not modeled, 15-25 Å separates the C-terminus of each N-domain and the N-terminus of the large AAA+ domain to which it connects.
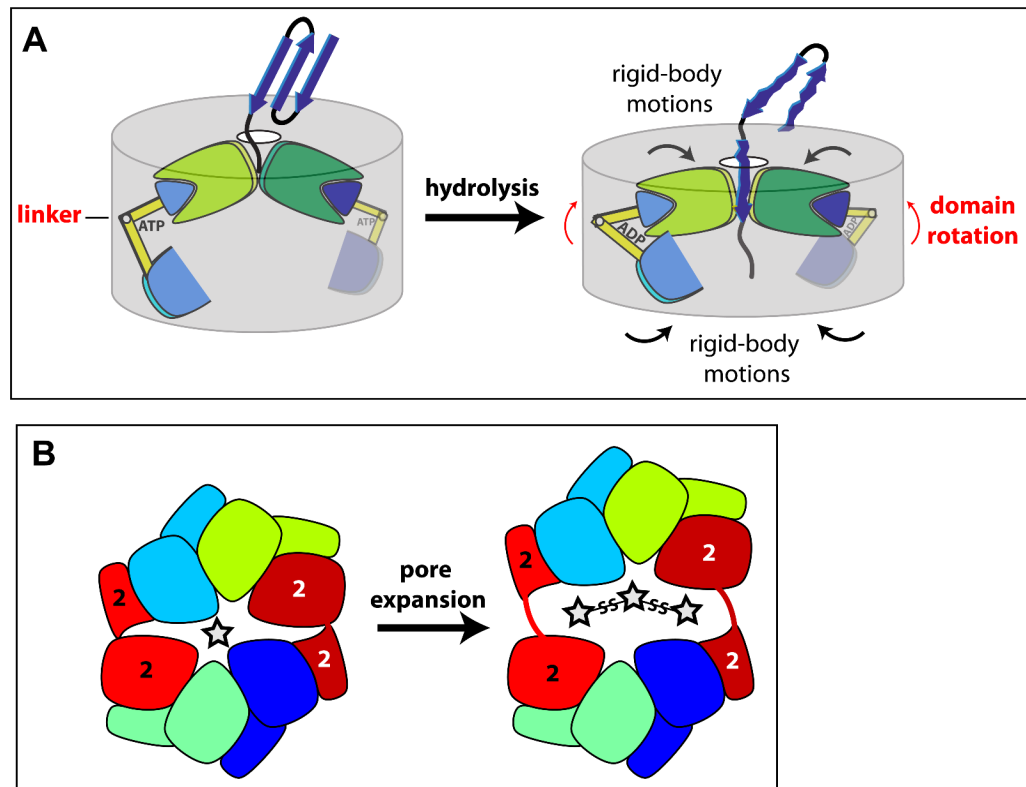
Figure 6. Models for protein unfolding and pore expansion
(A) Cartoon showing how ATP hydrolysis might change rotations between the large and small AAA+ domains of two ClpX subunits. These domain-domain rotations, in turn, could drive rigid-body movements that result in unfolding and translocation of a bound native substrate. **(B)** The cartoon on the left shows that the ClpX hexamer can be viewed as consisting of two jaw-like elements. The main contacts between these jaws are formed by the interfaces between the large and small AAA+ domains of the type-2 subunits (red/dark red). Opening of these interfaces, as shown in the exaggerated right cartoon, provides a potential mechanism for pore expansion to accommodate large substrates, including those with multiple chains.

Table 1

Crystallographic statistics.

	Nucleotide-free pdb code 3HTE	Nucleotide-bound pdb code 3HWS
Data Collection and Processing		
Wavelength (Å)	0.979	0.979
Resolution (Å)	50.0 – 4.0 (4.14-4.0)	50.0-3.25 (3.37-3.25)
Space group	$P2_12_12_1$	$P2_12_12_1$
Total reflections	315774	190525
Unique reflections	21881	32170
Mean I/σI	55.0 (5.7)	23.7 (3.2)
	5.4 (48.8)	6.1 (57.1)
Completeness (%)	99.9 (100.0)	99.5 (100.0)
Redundancy	14.4 (14.9)	5.9 (6.0)
Refinement		
Resolution (Å)	50.0 – 4.0	45.0 – 3.25
R_{work} / R_{free}	0.274 / 0.311	0.243 / 0.282
Rmsd bond lengths (Å)	0.002	0.003
Rmsd bond angles (°)	0.520	0.687
Ramachandran Plot Statistics		
Favored / Allowed / Unfavorable (%)	97.1 / 2.5 / 0.4	97.8 / 2.1 / 0.1

Values in parentheses refer to the highest resolution shell.